Geochemical Perspectives Letters

4.46 Ga zircons anchor chronology of lunar magma ocean

J. Greer[1,2,3*], B. Zhang[4], D. Isheim[5], D.N. Seidman[5], A. Bouvier[6], P.R. Heck[1,2]

OPEN ACCESS

https://doi.org/10.7185/geochemlet.2334

Abstract

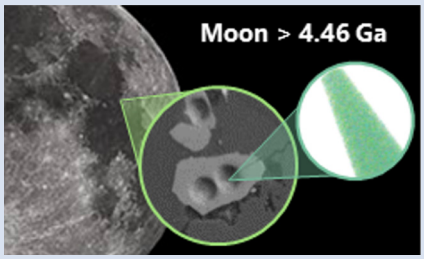

The crystallisation ages of lunar samples provide critical constraints on the minimum formation age of the Moon and its early evolution. Zircon crystals from Apollo 17 lunar impact melt breccia 72255 preserve ancient domains with a concordant average uranium-lead radiometric date of 4460 ± 31 Ma (Zhang *et al.*, 2021), the oldest lunar zircon yet reported. To assess the possible mobility of radiogenic lead in zircon, which may lead to redistribution and clustering of Pb atoms that may cause a U-Pb age bias (Valley *et al.*, 2014), we investigated a zircon grain from Zhang *et al.* (2021) by atom probe tomography (APT). The atomic spatial resolution analysis of individual mineral grains demonstrates the absence of nanoscale clustering of lead, which supports a 4.46 Ga ancient formation age for lunar zircon in sample 72255. This age pushes back the age of the first preserved lunar crust by ~40 Myr and provides a minimum formation age for the Moon within 110 Myr after the formation of the solar system.

Received 5 June 2023 | Accepted 18 September 2023 | Published 23 October 2023

Introduction

The leading hypothesis for the formation of the Earth–Moon system is the Giant Impact hypothesis where a Mars-sized object collided with the growing proto-Earth (Cameron and Ward, 1976; Canup, 2004), which may have resulted in a globally molten Moon known as the lunar magma ocean (LMO; Wood *et al.*, 1970; Warren, 1985). The LMO model explains the proposed structure of the lunar interior, with dense mafic materials forming the mantle (the source of mare basalts), ferroan anorthosite forming the crust, and a residual liquid with high concentrations of incompatible elements potassium, rare-earth elements, and phosphorus (KREEP) crystallising between the two (Warren, 1985). The density difference between some crustal materials (ilmenite-bearing cumulates) and mantle materials caused a so-called mantle overturn, which allowed magmas to intrude the anorthositic crust forming the plutonic Mg-suite rocks (Shearer *et al.*, 2015).

The timing of the Giant Impact and LMO crystallisation is debated (Borg *et al.*, 2015). The ^{182}Hf-^{182}W radiogenic systematics (Thiemens *et al.*, 2019), Hf model ages of lunar zircons (Barboni *et al.*, 2017), and dynamical modelling (Bottke *et al.*, 2015) place the Moon-forming event early in the solar system's history, between 4.52 to 4.47 Ga. In contrast, lunar Pb model ages (Connelly and Bizzarro, 2016) and thermal modelling (Maurice *et al.*, 2020) place it in the range of 4.43 to 4.42 Ga. A precise lower age limit for LMO crystallisation is given in Nemchin *et al.* (2009), which reported a ^{207}Pb/^{206}Pb date of 4417 ± 6 Ma measured by sensitive high-resolution ion microprobe (SHRIMP) for a zircon grain from the Apollo impact melt breccia 72215. Later Giant Impact and LMO crystallisation are favoured by the concordant formation of the source of mare basalts, selected ferroan anorthosites, Mg-suite rocks, and zircons (primarily derived from the Mg-suite) at ~4.3 Ga (Borg *et al.*, 2015).

The vast majority of lunar zircon crystallisation was likely part of, or post-dated, the urKREEP – the primordial KREEP component – because of the enrichment in incompatible elements (those remaining in the melt until the last rock suite is solidified) needed to form this mineral (*e.g.*, Warren and Wasson, 1979), and therefore occurred at, and after, the late stage of the LMO crystallisation. The U-Pb system in zircon is a particularly robust chronometer, as zircon readily incorporates U and excludes Pb from crystal lattices, and zircon is a refractory mineral both structurally and geochemically resistant to post-crystallisation thermal alteration (Finch and Hanchar, 2003). The U-Pb chronology of the oldest lunar zircon would thus provide constraints on the LMO crystallisation and the minimum timing of the Giant Impact.

Zhang *et al.* (2021) reported the U-Pb isotopic composition of 21 zircon grains measured with nanoscale secondary ionisation mass spectrometry (NanoSIMS) on a total of 42 spots in the Apollo 17 72255 Civet Cat norite clast (Meyer, 2009). The euhedral and subhedral zircon grains in this sample are small (10 to 25 μm in length; Fig. 1). The oldest six spots on these zircon

1. Robert A. Pritzker Center for Meteoritics and Polar Studies, Negaunee Integrative Research Center, Field Museum of Natural History, 1400 South DuSable Lake Shore Drive, Chicago, Illinois 60605-2496, USA
2. Department of the Geophysical Sciences, University of Chicago, 5734 South Ellis Avenue, Chicago, Illinois 60637-1468, USA
3. School of Geographical & Earth Sciences, University of Glasgow, G12 8QQ, Glasgow, UK
4. Department of Earth, Planetary, and Space Sciences, University of California, 595 Charles Young Dr. E, Los Angeles, California 90095-1567, USA
5. Northwestern University Center for Atom Probe Tomography, Department of Materials Science and Engineering, Northwestern University, 2220 Campus Drive, Evanston, Illinois 60208-3108, USA
6. Bayerisches Geoinstitut, Universität Bayreuth, Universitätsstraße 30, 95447 Bayreuth, Germany
* Corresponding author (e-mail: Jennika.Greer@glasgow.ac.uk)

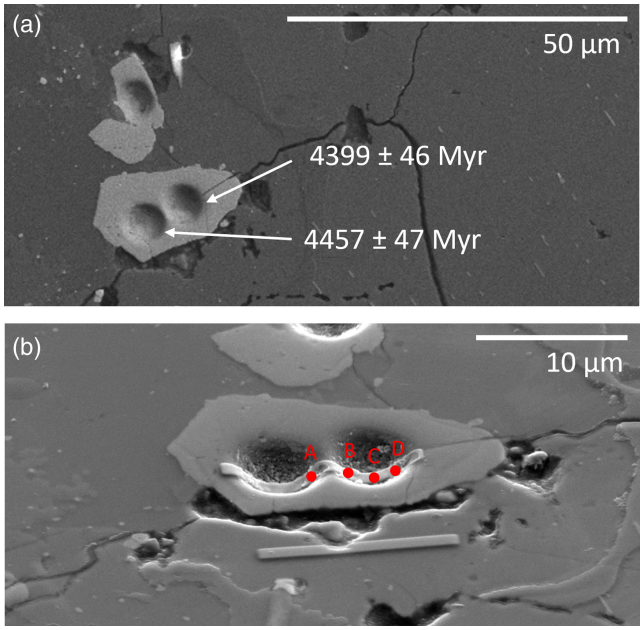

Figure 1 Secondary electron images of zircon Z14. **a)** Top-down image showing SIMS pits, **b)** image tilted at 55°, showing zircon with Pt deposit to be lifted out. The approximate positions of the sampling locations (A to D shown in red) for the successful APT runs are labelled. Scale bars shown.

grains have a concordant U-Pb average date of 4460 ± 31 Ma and define a weighted mean $^{207}Pb/^{206}Pb$ date of 4453 ± 34 Ma (all 2σ uncertainties). These dates have the potential to constrain the lower limit of the timing of the Giant Impact and LMO crystallisation at 4460 Ma. These ancient zircon dates reported by Zhang *et al.* (2021) could result either from unsupported Pb clusters caused by radiogenic Pb mobilisation or from Pb-retention domains that survived normal Pb loss. In the former scenario, radiogenic Pb mobilisation could compromise the authenticity of zircon U-Pb dates (Kusiak *et al.*, 2013a,b; Ge *et al.*, 2019), while in the latter, the widespread U-Pb dates of the Civet Cat norite zircons are due to normal Pb loss in some of the crystal domains (Arcuri *et al.*, 2020).

Methods

We used atom-probe tomography (APT), a time-of-flight mass spectrometry method with nanoscale spatial resolution, to investigate the Pb spatial distribution within an old lunar zircon domain to test if the ancient zircon dates in the Civet Cat norite obtained by Zhang *et al.* (2021) are authentic or potentially affected by nanoscale redistribution and clustering processes. Because zircon Z14 ($^{207}Pb/^{206}Pb$ date = 4453 ± 34 Ma, Th/U ≈ 7.2) has one of the six oldest domains in the Civet Cat norite, we selected it for APT analysis to investigate its Pb distribution at the nanoscale. During APT analyses, surface atoms of a sample nanotip are field-evaporated in a high electric field thermally activated by picosecond laser pulses and analysed with a position-sensitive time-of-flight mass spectrometer, yielding 3-D atom-by-atom distributions of elements and their isotopes with nanoscale spatial resolution (Fig. 2).

APT has been used in conjunction with secondary ion mass spectrometry (SIMS) to investigate Pb mobility at the nanoscale and reliably date 4.4 Ga Hadean zircon from Jack Hills (Valley *et al.*, 2014; Valley *et al.*, 2015) and 3.8 Ga Archean zircons from Beartooth Mountains (Blum *et al.*, 2018); other studies have used APT to look at lunar Pb-bearing minerals (*i.e.* Blum *et al.*, 2019; White *et al.*, 2019). Valley *et al.* (2014) demonstrated that nanoscale Pb clustering is associated with Y clustering, which is the result of the enrichment of less compatible elements after the formation of the zircon given sufficient atomic mobility. The Pb clusters detected in these samples, while demonstrating heterogeneity in Pb distribution, are much smaller than the size of the SIMS pit used to date the zircon (clusters are ~10 nm in diameter whereas pits produced by the SIMS primary beam have diameters of 5 to 10s of µm) and are therefore homogenous when averaged over the scale of the SIMS analysis. APT has several orders of magnitude greater spatial resolution (near-atomic) than the previous analyses of this zircon using NanoSIMS, which for this analysis

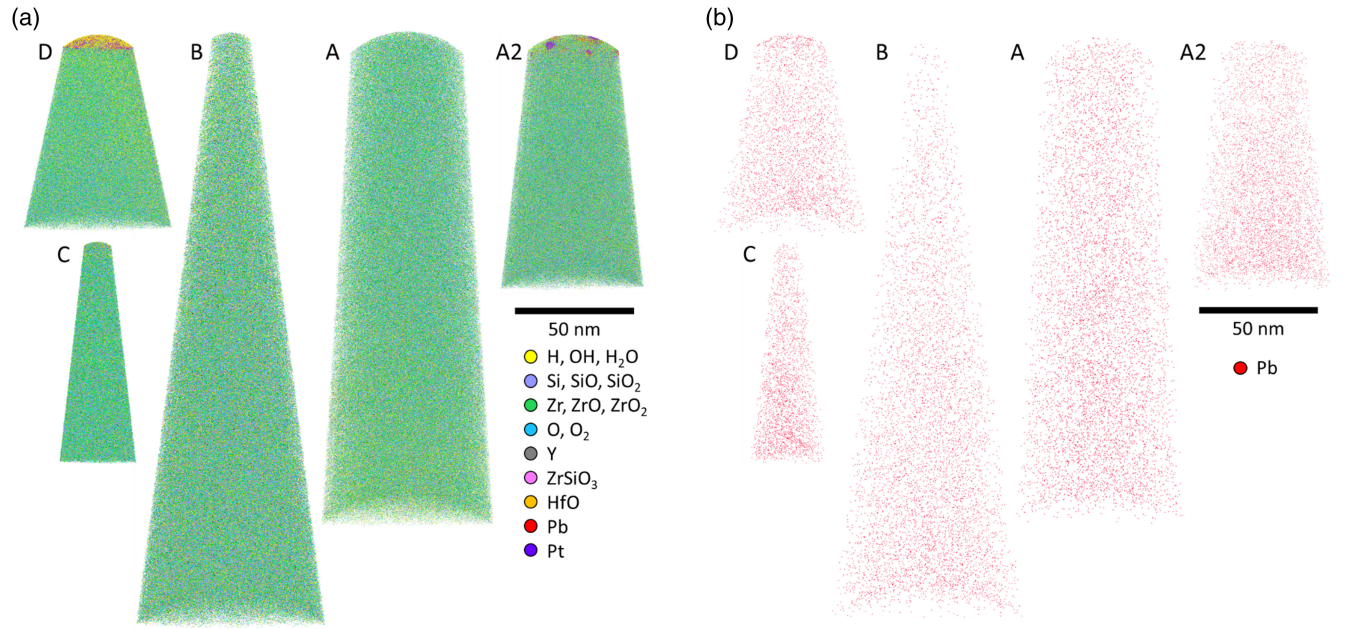

Figure 2 APT reconstructions of the nanotips. **a)** Shows the major ionic species present, with each ion identified as an individual point and colour coded, and **b)** shows just $^{208}Pb^{++}$ in red.

produced a pit size of a few μm across to analyse a statistically significant number of atoms to produce a date.

Details on the sample preparation methods and analytical conditions can be found in the supplementary information.

Results

A total of five nanotips were successfully produced from a lamella of zircon Z14 lifted out of two pits (Fig. 1, Fig. S-1) produced by NanoSIMS analyses. The nanotips were shaped to sample a volume immediately adjacent to the material analysed by NanoSIMS, and as to not include material that had been amorphised due to the primary ion beam damage created by the NanoSIMS, the nanotips were instead extracted from a depth of several hundreds of nanometres beneath the analysed surface. Species that were detected in APT include the major elements in zircon (Zr, Si, O), Y, Hf, Pb, Th, H, and oxide/hydride molecular ions (Fig. 2, Fig. S-2). The only isotope of Pb detected above background is $^{208}Pb^{2+}$, which can be used as a proxy for all Pb radiogenic isotopes as they are expected to exhibit the same chemical behaviour during secondary alteration processes such as shock metamorphism (*e.g.*, Deutsch and Schärer, 1990). In the 3D tomographic reconstructions of the datasets, we found no evidence of clustering of Pb, Y, or any other elements. We used the nearest neighbour distribution analysis (Stephenson *et al.*, 2007), one of the most robust ways to assess heterogeneity in concentration, including clustering. In the nearest neighbour analysis, each Pb atom was examined for the closest distance to the next Pb atom, and the frequency distribution of the distances was plotted (red, Fig. 3). This was then compared to a randomised distribution of points (black, Fig. 3) with the same volume concentration as in the dataset. This method is very sensitive to any type of inhomogeneity as concentration gradients would cause broadening of the distributions (Stephenson *et al.*, 2007).

Validating the Oldest Lunar Zircon Age

All datasets had prominent 104 Da peaks ($^{208}Pb^{2+}$) above background. There is an isobaric overlap at 104 Da with $^{28}Si_2{}^{16}O_3{}^+$. However, other peaks associated with this molecular ion (*e.g.*, $^{28}Si^{29}Si^{16}O_3{}^+$ at 105 Da) in the terrestrial/lunar abundance pattern are not present. Instead, the isotopic pattern of 105–110 Da matches that of the distribution of $Zr^{16}O^{2+}$ molecular species, which does not overlap with the 104 Da peak. Therefore, we conclude that the 104 Da peak is $^{208}Pb^{2+}$. Even in hypothetical samples where the peak at 104 Da would represent the combined concentration of $^{208}Pb^{2+}$ and $^{28}Si_2{}^{16}O_3{}^+$, any Pb clustering, if present, would be observable in the dataset from the combined peak if the Pb signal which contributes to the 104 Da peak is above background. Additionally, we determined our method is robust and not sensitive to the peak brackets or windows (referred to as the *peak ranges* in APT), for which Pb abundances are determined; ranging does not affect the result of the nearest neighbour distribution and clustering (Fig. S-3).

Valley *et al.* (2015) reported correlated clustering for both the Pb and Y distributions. The most prominent Y peak occurs at 29.67 Da, corresponding to $^{89}Y^{3+}$. While only Tip A has this Y peak above background (Fig. S-4), there are no major overlaps at this position, so this determination is unambiguous. In Valley *et al.* (2015), the Y clusters were more prominent than the Pb clusters and thus can be used as a proxy when Pb concentration is low. In addition, even if $^{28}Si_2{}^{16}O_3{}^+$ significantly contributes to the signal at 104 Da, the absence of Y clusters (Fig. 4) at the overlap-free 29.67 Da peak implies that there is no Pb clustering, thus demonstrating that the zircon is homogenous on the nanoscale for all

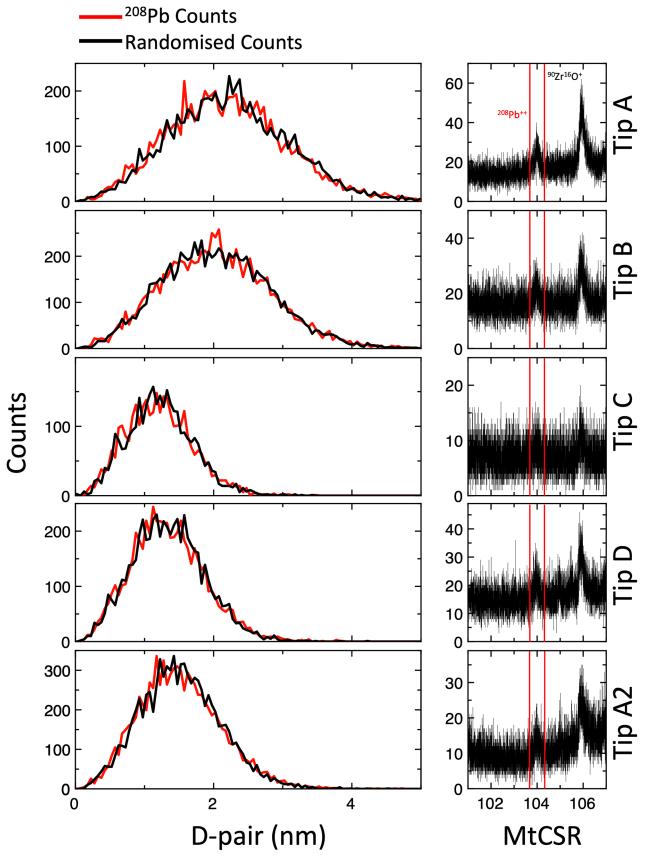

Figure 3 Nearest neighbour distribution of ^{208}Pb for all analysed tomographic datasets. To the left are the distributions of Pb atoms (shown as distance between pairs; D-pair) in the sample (red) and randomised distributions (black). On the right are plots of mass spectra of each of the 5 datasets for the mass-to-charge-state ratio (MtCSR) range around $^{208}Pb^{2+}$. The red dashed lines define the range of the Pb peak that was included in the nearest neighbour calculation.

detected species. While the absence of clustering in one dataset may suggest a larger inter-cluster distance compared to the sampled volume, it is noteworthy that none of the sampled volumes display any clusters (Fig. 3). This observation remains consistent even when the volumes are separated by distances of 1–2 μm, indicating the absence of nanoscale clustering within the analysed domain of this zircon (a volume that spans ~7 μm across the zircon and comprises a total analysed volume of ~1 μm in length, larger than the NanoSIMS spot size of ~5 μm).

There are heterogeneities in the Pb distribution at the microscale, as shown by Zhang *et al.* (2021); however, this cannot be due to the mixing of Pb nanoclusters. NanoSIMS analyses that report younger dates sampled domains with Pb-loss which occurred post-crystallisation, while the oldest dates sampled domains where radiogenic Pb was retained. The other explanation for these ancient dates, the presence of clusters of radiogenic Pb due to mobilisation, is ruled out by our APT analyses. We conclude that the weighted average date of 4460 ± 31 Ma (2σ) obtained for these zircons corresponds to its crystallisation age. Therefore, the minimum formation age of this old zircon population is the oldest evidence found to date for lunar zircon crystallisation.

Anchoring the Age of the Moon

Lunar silicate samples show ^{182}W excesses due to the decay of ^{182}Hf (with a half-life of ~8.9 Myr), and because of this, the

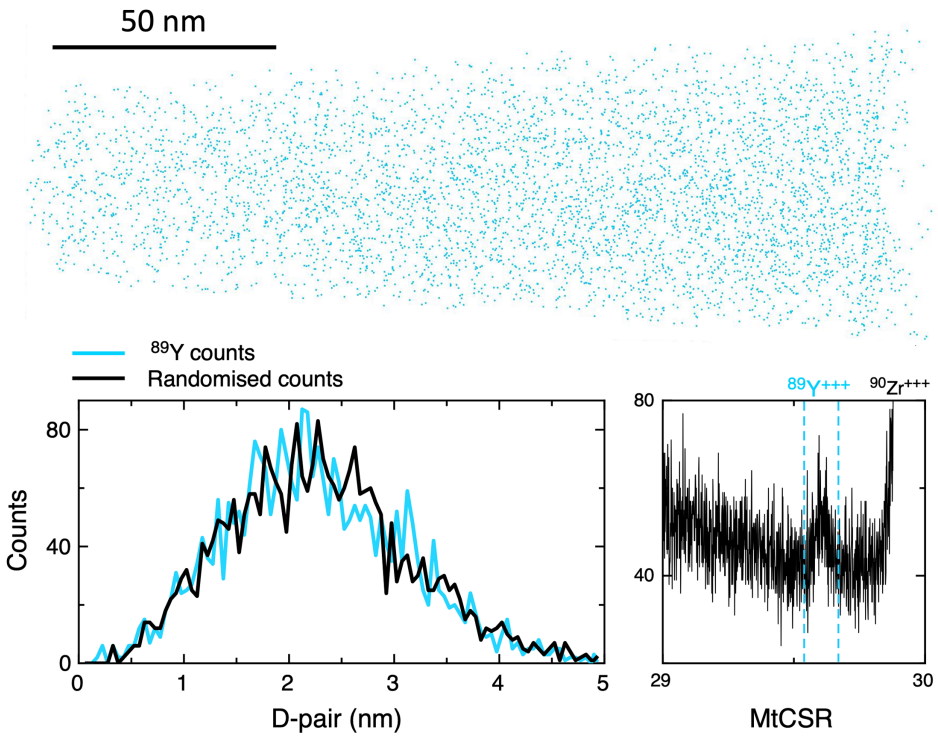

Figure 4 Reconstruction and nearest neighbour distribution of Y (shown as distance between pairs; D-pair) for Tip A. The top image shows the $^{89}Y^{3+}$ ions' individual points in blue. To the bottom left are the distributions of Y atoms in the sample (plotted in light blue) and randomised distribution (plotted in black). To the bottom right is a plot of the mass-to-charge-state ratio (MtCSR) at the range around $^{89}Y^{3+}$. The blue dashed line defines the range of the Pb peak that was included in the nearest neighbour calculation.

Moon should have formed at ~4.51 Ga (Thiemens *et al.*, 2019). Thermal modelling by Elkins-Tanton *et al.* (2011) suggests that lunar differentiation took place rapidly, with 80 vol. % of the LMO solidified within thousands of years. With this timeframe, the Civet Cat norite zircon age (4.46 Ga) given by Zhang *et al.* (2021) is a strong indication that the LMO had largely solidified by then. The $^{207}Pb/^{206}Pb$ date of the zircon (4.42 Ga) from Apollo 72215 likely points to the formation of the evolved, late-forming alkali suite in the lunar crust (Nemchin *et al.*, 2009). The concordant formation ages for the source of mare basalts, some ferroan anorthosites and Mg-suite rocks, and numerous zircons at ~4.3 Ga may mark a secondary large-scale event on the near side of the Moon. Subsequent bombardment events reworked or melted the earliest crust, modifying parts of the Civet Cat norite zircons, while pristine domains were preserved. The significance of the 4.46 Ga age holds on the preservation of domains within a grain despite post-crystallisation processes; such preservation is demonstrated by nanoscale analyses.

These findings require pushing the timing of the solidification of the lunar crust to within at least the first 100 Myr of the formation of the solar system and provide a minimum age for the Giant Impact event that formed the Earth-Moon system. Together with ^{182}Hf-^{182}W isotopic evidence that the core-mantle differentiation of the Moon occurred ~50 Myr after the formation of the solar system (Thiemens *et al.*, 2019), we can now place an age bracket on the timing of the Giant Impact, subsequent LMO crystallisation and the onset of Mg-suite magmatism to between 4.51 and 4.46 Ga. This serves as an anchoring age interval for the onset of the intense gravitational effects that the early, much closer Moon had on the young Earth, as well as when the Moon began recording a history of bombardments.

Acknowledgements

We are indebted to the NASA Apollo program and astronauts for collecting the samples, and to Ryan Zeigler and the curation team of NASA Johnson Space Center for allocating the lunar samples used in this research. JG acknowledges funding from the Field Museum's Women's Board Women in Science Graduate Fellowship. PRH acknowledges funding from the TAWANI Foundation. BZ's work is supported by NASA grants 80NSSC19K1238 and 80NSSC23K0035. Atom-probe tomography was performed at the Northwestern University Center for Atom-Probe Tomography (NUCAPT). The LEAP tomograph at NUCAPT was purchased and upgraded with grants from the NSF-MRI (DMR-0420532) and ONR-DURIP (N00014-0400798, N00014-0610539, N00014-0910781, N00014-1712870) programs. NUCAPT received support from the MRSEC program (NSF DMR-2308691) at the Materials Research Center, the SHyNE Resource (NSF ECCS-2025633), and the Initiative for Sustainability and Energy (ISEN) at Northwestern University. We also thank the constructive reviews from an anonymous reviewer and editor Romain Tartèse.

Editor: Romain Tartèse

Additional Information

Supplementary Information accompanies this letter at https://www.geochemicalperspectivesletters.org/article2334.

Cite this letter as: Greer, J., Zhang, B., Isheim, D., Seidman, D.N., Bouvier, A., Heck, P.R. (2023) 4.46 Ga zircons anchor chronology of lunar magma ocean. *Geochem. Persp. Let.* 27, 49–53. https://doi.org/10.7185/geochemlet.2334

References

Arcuri, G.A., Moser, D.E., Reinhard, D.A., Langelier, B., Larson, D.J. (2020) Impact-triggered nanoscale Pb clustering and Pb loss domains in Archean zircon. *Contributions to Mineralogy and Petrology* 175, 1–13. https://doi.org/10.1007/s00410-020-01698-w

Barboni, M., Boehnke, P., Keller, B., Kohl, I.E., Schoene, B., Young, E.D., McKeegan, K.D. (2017) Early formation of the Moon 4.51 billion years ago. *Science Advances* 3. https://doi.org/10.1126/sciadv.1602365

Blum, T.B., Reinhard, D.A., Chen, Y. Prosa, T.J., Larson, D.J., Valley, J.W. (2018) Uncertainty and sensitivity analysis for spatial and spectral processing of Pb isotopes in zircon by atom probe tomography. In: Moser, D.E., Corfu, F., Darling, J.R., Reddy, S.M., Tait, K. (Eds.) *Microstructural Geochronology: Planetary Records Down to Atom Scale*, American Geophysical Union, 327–350. https://doi.org/10.1002/9781119227250.ch16

Blum, T.B., Reinhard, D.A., Coble, M.A., Spicuzza, M.J., Chen, Y., Cavosie, A.J., Nasdala, L., Chanmuang, C., Prosa, T.J., Larson, D.J., Valley, J.W. (2019) A Nanoscale Record of Impact-Induced Pb Mobility in Lunar Zircon. *Microscopy and Microanalysis* 25, 2448–2449. https://doi.org/10.1017/S1431927619012972

Borg, L.E., Gaffney, A.M., Shearer. C.K. (2015) A review of lunar chronology revealing a preponderance of 4.34–4.37 Ga ages. *Meteoritics and Planetary Science* 50, 715–732. https://doi.org/10.1111/maps.12373

Bottke, W.F., Vokrouhlicky, D., Marchi, S., Swindle, T., Scott, E.R.D., Weirich, J.R., Levison, H. (2015) Dating the Moon-forming impact event with asteroidal meteorites. *Science* 348, 321–323. https://doi.org/10.1126/science.aaa0602

Cameron, A.G.W., Ward, W.R. (1976) The origin of the Moon. *Lunar and Planetary Science Conference* 7, 120.

Canup, R.M. (2004) Dynamics of lunar formation. *Annual Review of Astronomy and Astrophysics* 42, 441–475. https://doi.org/10.1146/annurev.astro.41.082201.113457

Connelly, J.N., Bizzarro, M. (2016) Lead isotope evidence for a young formation age of the Earth–Moon system. *Earth and Planetary Science Letters* 452, 36–43. https://doi.org/10.1016/j.epsl.2016.07.010

Deutsch, A., Schärer, U. (1990) Isotope systematics and shock-wave metamorphism: I. U-Pb in zircon, titanite and monazite, shocked experimentally up to 59 GPa. *Geochimica et Cosmochimica Acta* 54, 3427–3434. https://doi.org/10.1016/0016-7037(90)90295-V

Elkins-Tanton, L.T., Burgess, S., Yin, Q.-Z. (2011) The lunar magma ocean: Reconciling the solidification process with lunar petrology and geochronology. *Earth and Planetary Science Letters* 304, 326–336. https://doi.org/10.1016/j.epsl.2011.02.004

Finch, R.J., Hanchar. J.M. (2003) Structure and chemistry of zircon and zircon-group minerals. *Reviews in mineralogy and geochemistry* 53, 1–25. https://doi.org/10.1515/9781501509322-004

Ge, R., Wilde, S.A., Nemchin, A.A., Whitehouse, M.J., Bellucci, J.J., Erickson, T.M. (2019) Mechanisms and consequences of intra-crystalline enrichment of ancient radiogenic Pb in detrital Hadean zircons from the Jack Hills, Western Australia. *Earth and Planetary Science Letters* 517, 38–49. https://doi.org/10.1016/j.epsl.2019.04.005

Kusiak, M.A., Whitehouse, M.J., Wilde, S.A., Dunkley, D.J., Menneken, M., Nemchin, A.A., Clark, C. (2013a) Changes in zircon chemistry during Archean UHT metamorphism in the Napier Complex, Antarctica. *American Journal of Science* 313, 933–967. https://doi.org/10.2475/09.2013.05

Kusiak, M.A., Whitehouse, M.J., Wilde, S.A., Nemchin, A.A., Clark C. (2013b) Mobilization of radiogenic Pb in zircon revealed by ion imaging: Implications for early Earth geochronology. *Geology* 41, 291–294. https://doi.org/10.1130/G33920.1

Maurice, M., Tosi, N., Schwinger, S., Breuer, D., Kleine, T. (2020) A long-lived magma ocean on a young Moon. *Science advances* 6. https://doi.org/10.1126/sciadv.aba8949

Meyer, C. (2009) Lunar Sample Compendium. Astromaterials Research & Exploration *Science*, National Aeronautics and Space Administration, https://curator.jsc.nasa.gov/lunar/lsc/.

Nemchin, A., Timms, N., Pidgeon, R., Geisler, T., Reddy, S., Meyer, C. (2009) Timing of crystallization of the lunar magma ocean constrained by the oldest zircon. *Nature Geoscience* 2, 133–136. https://doi.org/10.1038/ngeo417

Shearer, C.K., Elardo, S.M., Petro, N.E., Borg, L.E., McCubbin, F.M. (2015) Origin of the lunar highlands Mg-suite: An integrated petrology, geochemistry, chronology, and remote sensing perspective. *American Mineralogist* 100, 294–325. https://doi.org/10.2138/am-2015-4817

Stephenson, L.T., Moody, M.P., Liddicoat, P.V., Ringer, S.P. (2007) New techniques for the analysis of fine-scaled clustering phenomena within atom probe tomography (APT) data. *Microscopy and Microanalysis* 13, 448–463. https://doi.org/10.1017/S1431927607070900

Thiemens, M.M., Sprung, P., Fonseca, R.O.C., Leitzke, F.P., Münker, C. (2019) Early Moon formation inferred from hafnium–tungsten systematics. *Nature Geoscience* 12, 696–700. https://doi.org/10.1038/s41561-019-0398-3

Valley, J.W., Cavosie, A.J., Ushikubo, T., Reinhard, D.A., Lawrence, D.F., Larson, D.J., Clifton, P.H., Kelly, T.F., Wilde, S.A., Moser, D.E., Spicuzza, M.J. (2014) Hadean age for a post-magma-ocean zircon confirmed by atom-probe tomography. *Nature Geoscience* 7, 219–223. https://doi.org/10.1038/ngeo2075

Valley, J.W., Reinhard, D.A., Cavosie, A.J., Ushikubo, T., Lawrence, D.F., Larson, D.J., Kelly, T.F., Snoeyenbos, D.R., Strickland, A. (2015) Nano- and micro-geochronology in Hadean and Archean zircons by atom-probe tomography and SIMS: New tools for old minerals. *American Mineralogist* 100, 1355–1377. https://doi.org/10.2138/am-2015-5134

Warren, P.H., Wasson, J.T. (1979) The origin of KREEP. *Reviews of Geophysics* 17, 73–88. https://doi.org/10.1029/RG017i001p00073

Warren, P.H. (1985) The magma ocean concept and lunar evolution. *Annual Review of Earth and Planetary Sciences* 13, 201–240. https://doi.org/10.1146/annurev.ea.13.050185.001221

White, L.F., Moser, D.E., Tait, K.T., Langelier, B., Barker, I., Darling, J.R. (2019) Crystallization and impact history of a meteoritic sample of early lunar crust (NWA 3163) refined by atom probe geochronology. *Geoscience Frontiers* 10, 1841–1848. https://doi.org/10.1016/j.gsf.2018.11.005

Wood, J.A., Dickey, J.S., Jr., Marvin, U.B., Powell, B.N. (1970) Lunar anorthosites and a geophysical model of the moon. *Proceedings of the Apollo 11 Lunar Science Conference 1*, 965–988.

Zhang, B., Lin, Y., Moser, D.E., Hao, J., Liu, Y., Zhang, J., Barker, I.R., Li, Q., Shieh, S.R., Bouvier, A. (2021) Radiogenic Pb mobilization induced by shock metamorphism of zircons in the Apollo 72255 Civet Cat norite clast. *Geochimica et Cosmochimica Acta* 302, 175–192. https://doi.org/10.1016/j.gca.2021.03.012

Geochemical Perspectives Letters

4.46 Ga zircons anchor chronology of lunar magma ocean

J. Greer, B. Zhang, D. Isheim, D.N. Seidman, A. Bouvier, P.R. Heck

Supplementary Information

The Supplementary Information includes:

- Methods
- Table S-1
- Figures S-1 to S-4
- Supplementary Information References

Methods

The zircon grain Z-14 used in this study measures 22 μm × 12 μm (Fig. 1), and was analysed for U-Pb systematics by Zhang *et al.* (2021) using NanoSIMS. The size of the grain presents some challenges in APT sample preparation. A strong bond to the substrate is essential as the mechanical stresses at the nanotip are large, and a weak point in a sample—such as a grain boundary— can lead to the fracture of a specimen during APT analyses (Kelly and Miller, 2007). A large thick base permits heat introduced by the laser to be more efficiently conducted away from the apex of a nanotip to its base. To avoid the presence of a grain boundary, the nanotips from this zircon need to be shorter than nanotips from larger zircon grains, such as those studied by Valley *et al.* (2014), to be certain that a grain boundary is not included. A lamella of approximately 1 μm × 10 μm was milled with a focused ion beam (FIB) microscope, lifted out (Fig. 1) using a micromanipulator, and subsections of the lamella are firmly attached to Si flat-topped posts with gas injection system (GIS)-deposited Pt. These subsections of the zircon are further milled to produce the nanotips (*e.g.*, Fig. S-1). The material within several nanometres from the surface could have been subjected to sputtering-induced amorphisation during NanoSIMS analyses (Aléon-Toppani *et al.*, 2021). Because of this, the nanotips were fabricated to exclude this zone using the FIB microscope to remove the top material by ion beam milling away the top material. The final FIB microscope sharpening steps are done at a low voltage (5 kV) to minimise the thickness of the damaged/amorphised zone produced by the FIB ion beam. For several of these samples, the APT analyses are significantly larger than the thickness of the amorphised layer (~20 nm), and no differences were noticed between the top of the nanotip that might have been affected by the ion beam and the lower parts of the reconstruction coming from a greater sample depth. Tips D and A2 preserve some of the Pt deposited during sample preparation at the apex.

In atom-probe tomography we apply a high electric field in conjunction with a pulsed picosecond UV laser (λ = 355 nm), which causes field-evaporation and -ionisation of atoms from a nanotip. The field-evaporated ions are then accelerated through a local electrode and detected by a position-sensitive microchannel plate. This method yields both the elemental and isotopic identities and spatial distribution of the atoms in a sample. We used a CAMECA LEAP 5000-

XS equipped with a picosecond UV laser, with a laser pulse energy of 50 or 200 pJ and a pulse repetition rate of 200 kHz. A total of six nanotips were prepared and analysed from zircon Z-14. Tips A, B, and C were located in the righthand NanoSIMS spot (Fig. 1) which yielded a $^{207}Pb/^{206}Pb$ date of 4399 ± 46 Myr, and Tips D, E, F were located in the lefthand NanoSIMS spot which yielded a $^{207}Pb/^{206}Pb$ date of 4453 ± 47 Myr. The first two nanotips (Tips E, F) were unsuccessful, and fractured before steady-state evaporation occurred. These nanotips were analysed with APT conditions (pulse energy of 200 pJ) which had been previously reported for zircon (*e.g.*, Valley *et al.*, 2014), but were unsuitable for these samples. Of the four successful nanotips, all were analysed with a laser pulse energy of 50 pJ. The run for Tip A was stopped manually, then resharpened and reanalysed as Tip A2 (Table S-1). Since resistive materials like zircon can have many different species of complex molecular ions in their mass spectra (*e.g.*, Valley *et al.*, 2015), the conditions for our analyses were chosen to minimise the presence of molecular ions.

Supplementary Tables

Table S-1 Summary of the analytical conditions for APT and yields from the zircon nanotips.

Tip Name	Temperature (K)	Pulse Energy (pJ)	Pulse Rate (kHz)	Total # of detections	Length of tip (nm)
F	50	200	200	n/a	n/a
E	50	200	200	n/a	n/a
D	30	50	200	~14.5 M	~70
C	50	50	200	~7.5 M	~90
B	50	50	200	~18.3 M	~240
A	30	50	200	~31.6 M	~200
A2	30	50	200	~15.0 M	~100

Supplementary Figures

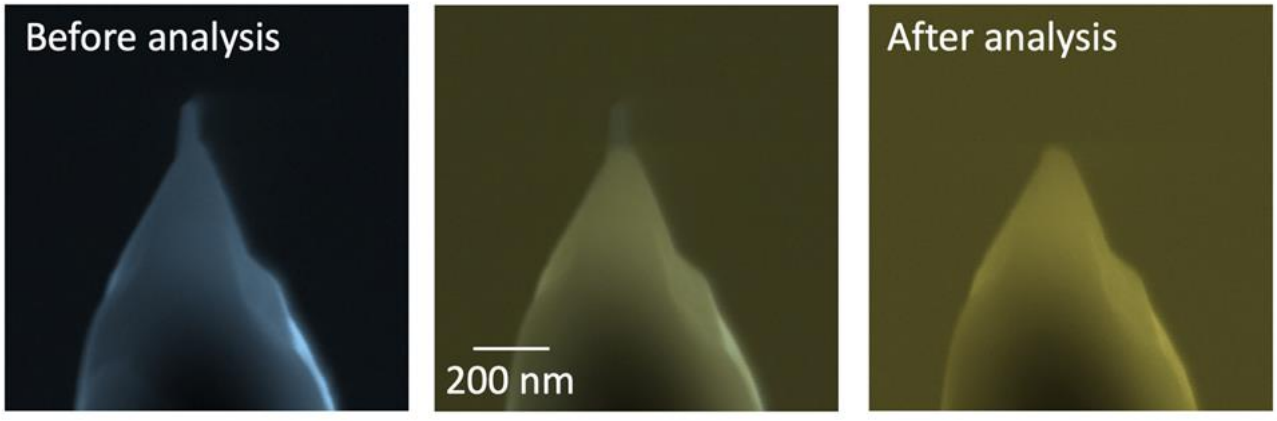

Figure S-1 False-colour SEM images of a Tip A before (left) and after (right) APT analysis, and a composite image in the middle to highlight the amount of material field-evaporated during the APT analysis. After APT analysis, this sample was later re-sharpened to produce Tip A2.

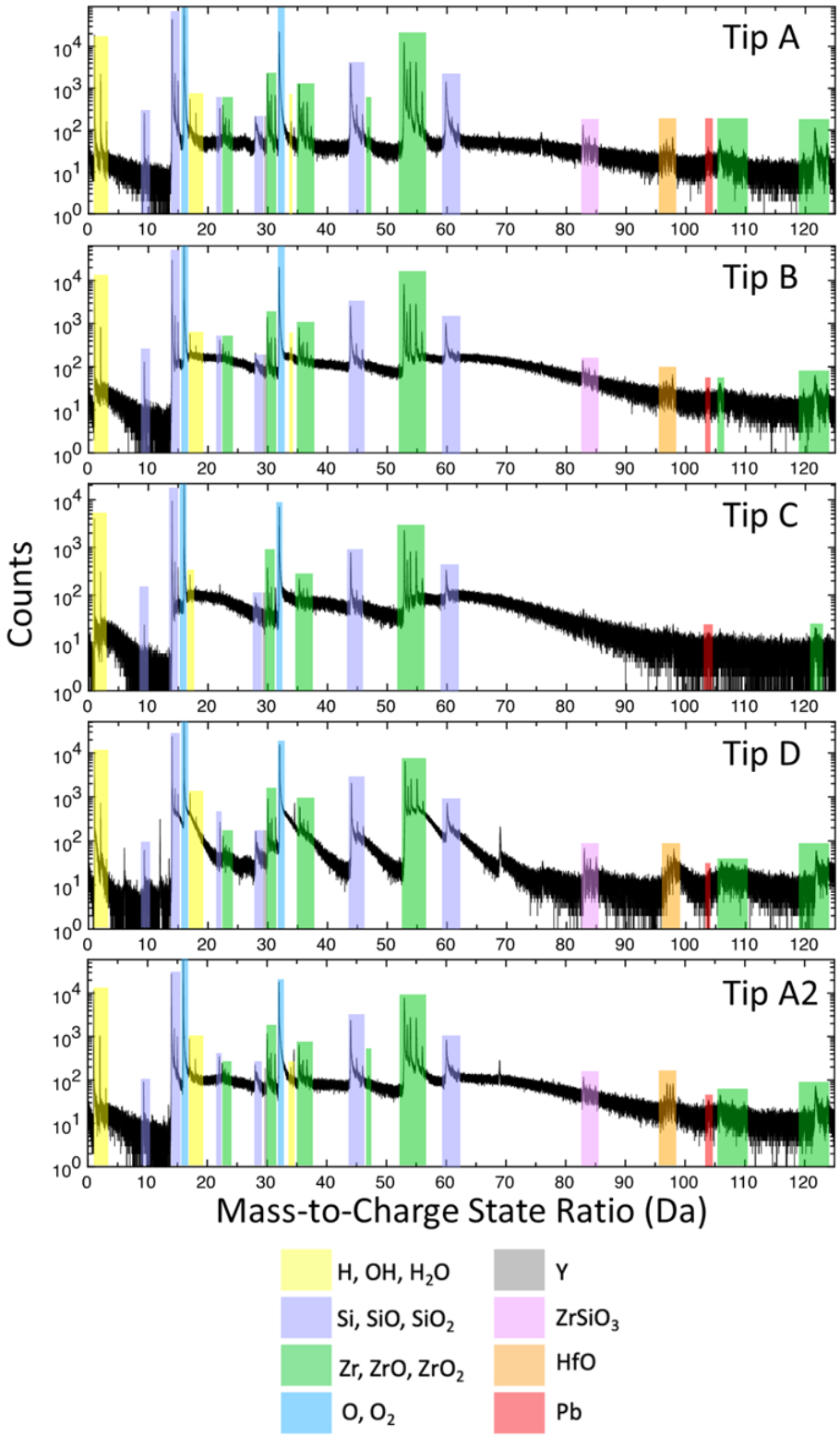

Figure S-2 Mass-to-Charge State Ratio spectra for the 5 nanotips analysed. Important species have been labelled with a corresponding colour. This can include singly, doubly, and triply charged species, as well as complex ions.

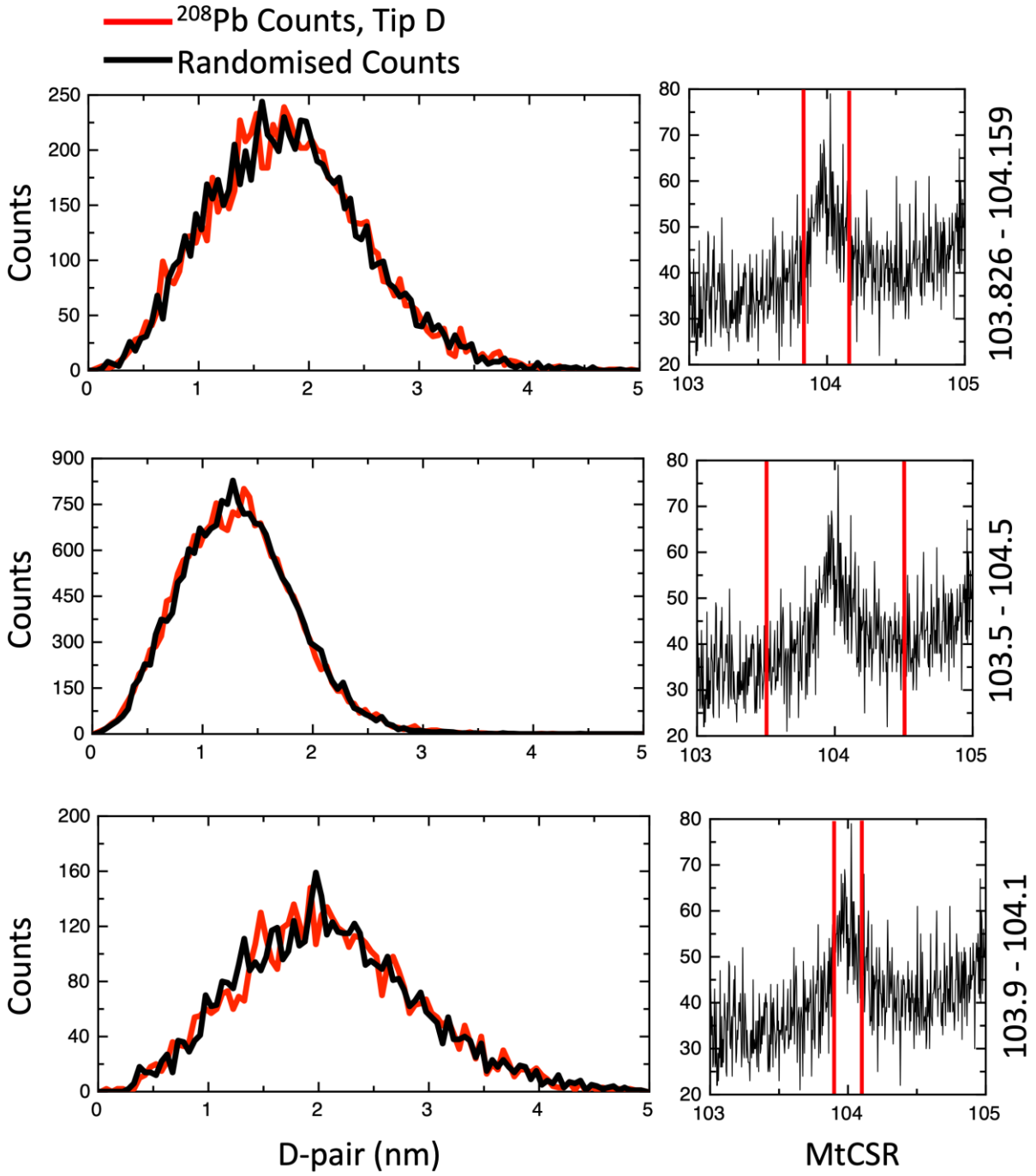

Figure S-3 Nearest neighbour distribution plots with different ranges, showing there is no clustering regardless of how Pb is ranged. The distribution of Pb atoms in the sample (red) and random distribution (black) is plotted to the left. On the right are the mass-to-charge State ratio (MtCSR) spectra showing the range (bracketed by red lines) that was plotted in the left.

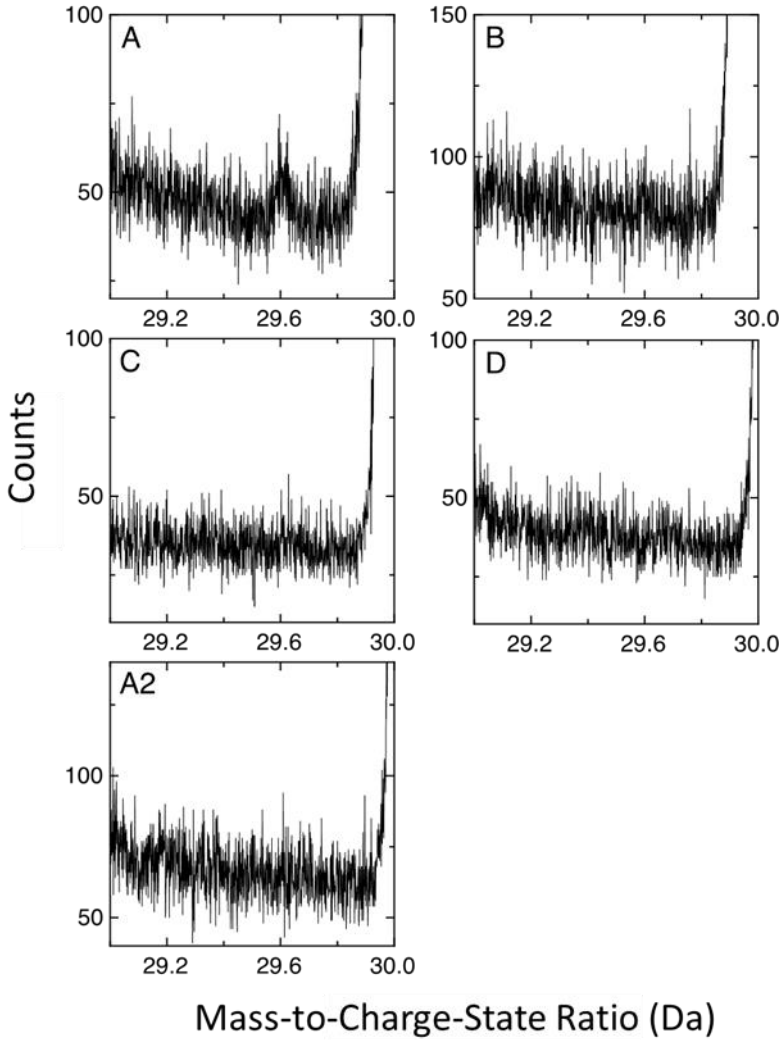

Figure S-4 Mass-to-charge-state ratio spectra for the 5 nanotips analysed between 29 and 30 Da. Only one nanotip, Tip A, shows a peak at 29.67 Da, corresponding to $^{89}Y^{3+}$.

Supplementary Information References

Aléon-Toppani, A., Brunetto, R., Aléon, J., Dionnet, Z., Rubino, S., Levy, D., Troadec, D., Brisset, F., Borondics, F., Brisset, F. (2021) A Preparation Sequence for Multi-Analysis of Micrometer-Sized Extraterrestrial Samples. *Meteoritics and Planetary Science* 56, 1151-1172. https://doi.org/10.1111/maps.13696

Kelly, T.F., Miller, M.K. (2007) Atom probe tomography. *Review of Scientific Instruments* 78, 031101. https://doi.org/10.1063/1.2709758

Valley, J.W., Cavosie, A.J., Ushikubo, T., Reinhard, D.A., Lawrence, D.F., Larson, D.J., Clifton, P.H., Kelly, T.F., Wilde, S.A., Moser, D.E., Spicuzza, M.J. (2014) Hadean age for a post-magma-ocean zircon confirmed by atom-probe tomography. *Nature Geoscience* 7, 219-223. https://doi.org/10.1038/ngeo2075

Valley, J.W., Reinhard, D.A., Cavosie, A.J., Ushikubo, T., Lawrence, D.F., Larson, D.J., Kelly, T.F., Snoeyenbos, D.R., Strickland, A. (2015) Nano-and micro-geochronology in Hadean and Archean zircons by atom-probe tomography and SIMS: New tools for old minerals. *American Mineralogist* 100, 1355-1377. https://doi.org/10.2138/am-2015-5134

Zhang, B., Lin, Y., Moser, D.E., Hao, J., Liu, Y., Zhang, J., Barker, I.R., Li, Q., Shieh, S.R., Bouvier, A. (2021) Radiogenic Pb mobilization induced by shock metamorphism of zircons in the Apollo 72255 Civet Cat norite clast. *Geochimica et Cosmochimica Acta* 302, 175-192. https://doi.org/10.1016/j.gca.2021.03.012